

Ab Initio Models of Dislocations*

Emmanuel Clouet

Abstract This chapter reviews the different methodological aspects of the *ab initio* modeling of dislocations. Such simulations are now frequently used to study the dislocation core, *i.e.* the region in the immediate vicinity of the line defect where the crystal is so strongly distorted that an atomic description is needed. This core region controls some dislocation fundamental properties, like their ability to glide in different crystallographic planes. *Ab initio* calculations based on the density functional theory offer a predictive way to model this core region. Because dislocations break the periodicity of the crystal and induce long range elastic fields, several specific approaches relying on different boundary conditions have been developed to allow for the atomistic modeling of these defects in simulation cells having a size compatible with *ab initio* calculations. We describe these different approaches which can be used to study dislocations with *ab initio* calculations and introduce the different analyses which are currently performed to characterize the core structure, before discussing how meaningful energy properties can be extracted from such simulations.

1 Introduction

Dislocations are line defects which control the development of the plastic deformation in crystals. These defects induce a long range stress field, which is well described by elasticity, and dislocation elasticity theory offers a powerful framework to model dislocations and their interaction with their surrounding environment (Hirth and Lothe 1982; Bacon et al 1980). But some of their fundamental properties, like

Emmanuel Clouet

DEN-Service de Recherches de Métallurgie Physique, CEA, Université Paris-Saclay, F-91191 Gif-sur-Yvette, France, e-mail: emmanuel.clouet@cea.fr

* To appear in *Handbook of Materials Modeling*, W. Andreoni and S. Yips (Eds.)

their glide plane and their mobility, highly depend on their core, *i.e.* the region in the immediate vicinity of the defect where the perturbation of the crystal is too important to be described by elasticity. The modeling of this core region necessitates an atomic description and atomistic simulations have thus become a valuable tool to study dislocation properties. Among such simulations, *ab initio* calculations based on the density functional theory (DFT), as they rely on an electronic description of the atomic bonding, appear as the most accurate and predictive. But as these calculations are still limited in the size of the system they can handle, typically at most a few hundred atoms, the *ab initio* modeling of dislocations need special attention. Specific methodologies have been therefore developed to study dislocation core properties with *ab initio* calculations. The purpose of this chapter is to review the different modeling approaches for the *ab initio* study of dislocations, starting from a quick overview of DFT formalism, before describing more thoroughly boundary conditions specific to dislocation models, then the analysis of the atomic structure in the dislocation core and finally the extraction of meaningful energy properties. Beyond the examples illustrated in this chapter, results which have been obtained from such *ab initio* studies for the dislocation core properties in different metals and semi-conductors can be found in the recent review of Rodney et al (2017).

2 *Ab initio* calculations

Ab initio calculations describe the bonding between atoms thanks to the resolutions of the Schrödinger equation for the electrons of the system. These are first-principles approaches as they do not use any experimental data and allows the modeling of atomic interaction only from the atomic number and other fundamental quantities. Compared to empirical interatomic potentials, such approaches are completely transferable, without any parameterization depending on the environment under study, but at the expense of a much higher CPU time. Although *ab initio* in nature and usually very accurate, these approaches nevertheless rely on different approximations, the validity of which needs generally to be assessed.

The most fundamental approximation is the Born-Oppenheimer approximation. As atom nuclei have a much higher mass than electrons, one can assume that the electrons are always equilibrated with respect to the positions of the nuclei which are considered as immobile. The resolution of the Schrödinger equation for the electrons therefore leads to the energy of the system as a function of the atomic positions. Knowing this function and also its first derivatives, *i.e.* the atomic forces, standard algorithms of atomic simulations can then be used. For the *ab initio* modeling of dislocations, this is usually restricted to molecular statics, including energy barrier calculations, because of the high CPU burden of the energy and force calculation.

Most *ab initio* calculations of dislocations are relying on the density functional theory (DFT). This makes use of the Hohenberg and Kohn (1964) theorem showing that the ground-state energy is the minimum of a functional depending only on the electronic density. This dramatically simplifies the problem as the electronic density

depends only on the position, whereas the many-electron wave function entering Schrödinger equation is a function depending on the $3N$ electron coordinates, with N the number of electrons in the system. The Kohn and Sham (1965) approach allows then a practical implementation, where the Schrödinger equation is solved for an equivalent system of non-interacting electrons. This necessitates the definition of an unknown contribution to the Hamiltonian, the exchange and correlation potential. Most of dislocation calculations are performed with the local density (LDA) or the generalized gradient (GGA) approximations, assuming that this contribution depends only locally on the electronic density or also its gradient.

For dislocation calculations, it is enough to consider that only the electrons of the outer shells participate to the atomic bonding. Electrons of the inner shells are not sensitive to the atom environment and can be assumed to have the same ground state as for the isolated atom. Kohn-Sham equations are then solved only for valence electrons. One can further reduce the CPU overhead by replacing with a pseudopotential the interaction potential of the valence electrons with the ionic core. This pseudopotential aims to reduce the strong oscillations of the electronic wave functions close to the dislocation core, because the description of these oscillations necessitates a large basis set, while still leading to the correct wave functions outside this core region. Different pseudoization schemes, norm-conserving or ultrasoft pseudopotentials as well as the projected augmented wave (PAW) method, are available.

Ab initio codes used for dislocations are relying on Born-von Karman periodic boundary conditions to model the solid, whatever the boundary conditions used to incorporate a dislocation in the simulation cell (Section 3). Electronic wave functions are thus a superposition of Bloch waves with wavevectors spanning the first Brillouin zone. Integration in the reciprocal space is performed on a regular grid sampling the first Brillouin zone, using smearing functions to broaden the electronic density of states. Different basis sets can be used to describe the Bloch waves, with plane waves being the most popular choice for dislocations.

Ab initio approaches devoted to the study of dislocations are thus not specific: they are making use of standard DFT implementations which are now current modeling tools in solid state physics. Feature specific to dislocation modeling, as described in the next section, is the necessity to use a supercell large enough to let the dislocation core adopt its fully relaxed configuration, with boundary conditions compatible with the long range distortion induced by the defect. A high accuracy is also generally needed for such calculations as the energy variations involved by the dislocation core are usually small. For instance, the Peierls energy barrier opposing the glide of $1/2 \langle 111 \rangle$ screw dislocations in BCC transition metals does not exceed $100 \text{ meV}/b$, where b , the norm of the Burgers vector, corresponds to the height of the simulation cell necessary to model such a dislocation.

3 Boundary conditions

The *ab initio* modeling of dislocations needs special care in the way the boundary conditions are handled. First, a dislocation creates a long-range elastic field which needs to be taken into account. Second, it is not possible to include a single dislocation in a simulation box with full periodic boundary conditions which usually constitute the paradigm in the modeling of bulk materials: the dislocation opens a displacement discontinuity and another defect is needed to close the discontinuity and allow for periodicity. As a result, different boundary conditions compatible with *ab initio* calculations have been developed to model dislocations.

All approaches enforce periodicity in the direction of the dislocation line. In pure metals, one usually uses the shortest periodicity vector to define the dimension of the simulation cell in this direction, thus modeling an infinite straight dislocation. But this size needs to be increased if one wants to introduce a solute atom on the dislocation line, so as to minimize the interaction of the solute atom with its periodic images and truly study the interaction of the dislocation with a single foreign atom. A larger size is also needed to model a kinked dislocation. This is usually possible only in covalent crystals where the atomic bonds are highly directional, leading to abrupt kinks experiencing a non negligible energy barrier when migrating along the dislocation line. In metallic systems with less directional atomic bonding, kinks are usually spread over a larger distance and are highly mobile, making it hard to stabilize them in a simulation cell whose size is compatible with *ab initio* calculations.

3.1 Cluster approach

The easiest way to model a dislocation is to use an infinite cylinder whose axis coincides with the dislocation line. Periodicity is enforced only along the dislocation line. The dislocation is created by displacing all atoms according to the Volterra solution given by anisotropic elasticity theory for the dislocation displacement field (Stroh 1958, 1962). Atoms at the cylinder surface (region 2 in Fig. 1a) are kept fixed in their initial positions and only atoms inside the cylinder are relaxed. One thus models an isolated dislocation in an infinite continuum.

But this modeling approach has severe drawbacks. The elastic solution used to fix the atoms at the boundary is only approximate as it relies on linear elasticity, thus neglecting crystal anharmonicity which can be strong close to the dislocation line. Moreover, the Volterra elastic solution, used to fix the atoms at the boundary, only corresponds to the long-range elastic field of the dislocation. Close to the dislocation line some additional contributions, the dislocation core field, need to be accounted for (Eshelby et al 1953). A spreading of the dislocation core can be the reason for the existence of such a core field, but even dislocations with a compact core, like $\langle 111 \rangle$ screw dislocations in BCC metals, possess a non negligible core field. Although this core field decays more rapidly than the Volterra elastic field, the size of the

simulation boxes that can be handled by *ab initio* calculations are never large enough to neglect it. The rigid boundary conditions do not allow the correct development of this core field and thus perturb the relaxation of the dislocation core.

The fixed atomic positions imposed at the boundary also prevent use of this method to determine the lattice friction opposing dislocation motion. If the dislocation moves during the simulation, this boundary condition will not be compatible anymore with the new dislocation position. This induces indeed a back-stress opposing the dislocation motion. As a result, any simulation relying on this boundary condition will overestimate the dislocation Peierls stress, which is the minimum stress necessary to move the dislocation at 0 K.

3.2 Flexible boundary conditions

To remove the artifacts induced by the rigid boundary conditions, dislocation modeling with flexible boundary conditions has been developed. The proposed method relies either on the use of the lattice Green's function (Sinclair et al 1978; Woodward 2005) or on the coupling with an empirical potential (Liu et al 2007; Chen et al 2008).

The lattice Green's function $G_{ij}(\mathbf{r})$ expresses, in the crystal harmonic approximation, the displacement \mathbf{u} induced on an atom in position \mathbf{r} by a force \mathbf{F} acting on an atom at origin:²

$$u_i(\mathbf{r}) = G_{ij}(\mathbf{r})F_j. \quad (1)$$

This lattice Green's function can be obtained by inversion of the force-constant matrices of the perfect crystal (Yasi et al 2012; Tan and Trinkle 2016) or can be tabulated from direct calculations in a perfect lattice (Sinclair et al 1978; Rao et al

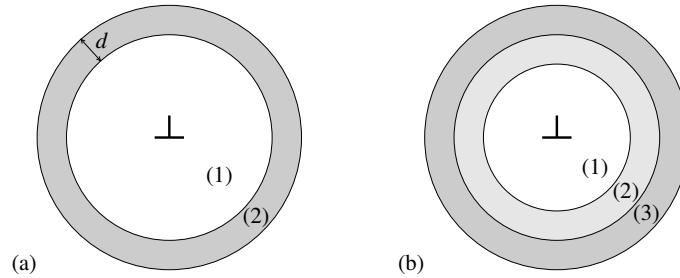


Fig. 1 Boundary conditions used to model an isolated straight dislocation in the cluster approach. The outer boundary is either (a) rigid or (b) flexible and controlled by lattice Green's functions or by coupling with an empirical potential.

² We use the Einstein implicit summation convention on repeated indexes appearing in all expressions.

1998). In the long range limit, $G_{ij}(\mathbf{r})$ converges to the elastic Green's function given by anisotropic elasticity theory.

Flexible boundary conditions based on lattice Green's functions still make use of a cylinder geometry to model a single dislocation, but three zones are now defined (Fig. 1b). Atoms in the inner zone (1) are relaxed with the *ab initio* code until the forces acting on them are smaller than a fixed threshold, while atoms in zones (2) and (3) are kept fixed. At the end of this step, atomic forces have appeared in zone (2), because the dislocation elastic field deviates from the Volterra solution used as an initial guess. The lattice Green's function is then used to displace atoms in all three zones according to Eq. 1 using all atomic forces in zone (2). This leads to the cancellation of forces in zone (2) but makes new forces appear in zone (1). The procedure is thus iterated until all forces in zones (1) and (2) are null. This self-consistent cycle is necessary because the lattice Green's function of the perfect crystal only approximates the linear response of the dislocated crystal. Atoms in zone (3) serve as a buffer to prevent any perturbation by the external boundary of forces building in zone (2). As shown by Segall et al (2003), this buffer region may need to be quite large in metals to obtain negligible perturbations in the inner regions. This can be minimized by removing the surfaces delineating zone (3) and using periodic boundary conditions in all directions. Interface defects are then present at the boundary between two periodic simulations cells. But these defects lead to a smaller perturbation of the electronic density than the vacuum layer of the surfaces (Woodward 2005). One thus perfectly models an isolated dislocation in an infinite crystal taking full account of the dislocation core field. It is possible to study dislocation cores with a reduced number of atoms in the simulation cell, a size usually compatible with *ab initio* calculations.

A similar approach relies on the coupling of the *ab initio* calculations with an empirical potential (Liu et al 2007; Chen et al 2008). The simulation cell is still divided in three regions (Fig. 1b). *Ab initio* calculations are performed only for a smaller simulation cell corresponding to regions (1) and (2). Atoms in regions (2) and (3) are relaxed according to the forces calculated with the empirical potential, whereas atoms in region (1) are relaxed according to *ab initio* forces plus a correction to withdraw the perturbation caused by the external boundary of the *ab initio* box. The buffer region (2) has been added to the original approach (Choly et al 2005) to minimize this correction by protecting atoms from the external boundary. To operate, this method needs therefore an empirical potential which perfectly reproduces the lattice parameters given by *ab initio* calculations, which can generally be done by rescaling the distances. Besides, the potential has also to match as best as possible the *ab initio* linear response, *i.e.* at least the elastic constants and, ideally, the whole phonon spectrum.

As it will be discussed in the last section, the main drawback of this *ab initio* dislocation model using flexible boundaries arises from the difficulty of extracting dislocation energy. The problem may be actually less sensitive with the second approach relying on a coupling with an empirical potential where an energy formulation exists. In this case, one can obtain a reasonable estimation of the dislocation energy provided the potential gives an accurate description of the boundary energy

compared to the *ab initio* calculations. While these flexible boundaries truly allow the modeling of an isolated dislocation, thus predicting its core structure and its evolution under an applied stress without any *a priori* artifact induced by the small size of the simulation cell inherent to *ab initio* calculations, the approach is still under active development to also provide information on the dislocation energy.

3.3 Periodic boundary conditions

To get rid of the external boundary and to use periodic boundary conditions in all three directions without the introduction of a defective interface, one needs to introduce in the simulation cell a dislocation dipole, *i.e.* two dislocations with opposite Burgers vectors. One thus models a 2D periodic array of dislocations (Fig. 2).

Several arrangements of dislocation arrays can be thought of, but they are not all equivalent. Among all of them, the ones which are quadrupolar display strong advantages. A periodic array is quadrupolar, if the vector \mathbf{d} linking the two dislocations of opposite signs is equal to $1/2 (\mathbf{u}_1 + \mathbf{u}_2)$, where \mathbf{u}_1 and \mathbf{u}_2 are the periodicity

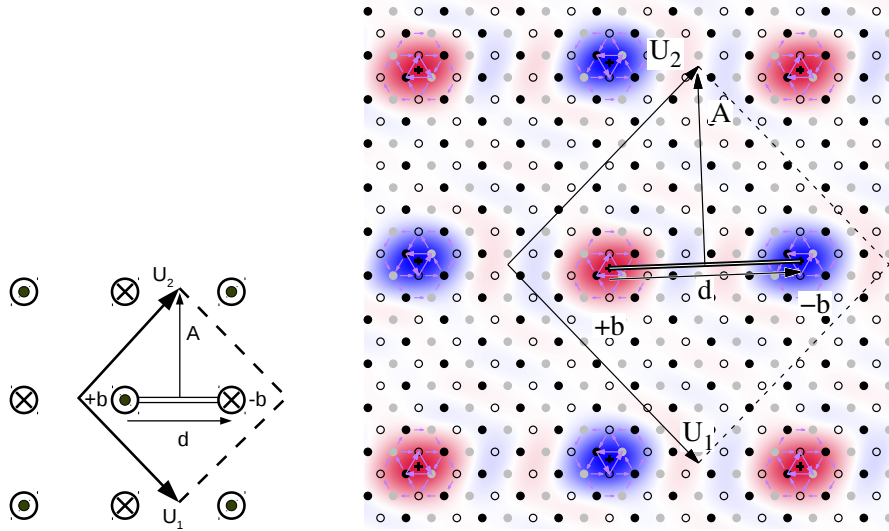


Fig. 2 Simulation of a dislocation dipole with periodic boundary conditions, using a quadrupolar arrangement. The dipole is defined by its Burgers vector \mathbf{b} , the dipole vector \mathbf{d} joining the two dislocation centers, and the cut vector \mathbf{A} , with the corresponding discontinuity surface indicated by a double black line. \mathbf{u}_1 and \mathbf{u}_2 are the periodicity vectors of the simulation cell perpendicular to the dislocation line. The example on the right corresponds to the simulation cell used for the modeling of the $1/2 \langle 111 \rangle$ screw dislocation in bcc iron. The dislocation core structures are shown through their differential displacement maps and their density (*cf.* Fig. 3a for a details).

vectors of the simulation cell (Fig. 2). This ensures that every dislocation is a symmetry center of the array: fixing, as a convention, the origin at a dislocation center, if a dislocation \mathbf{b} is located at the position \mathbf{r} , there will also be a dislocation \mathbf{b} in $-\mathbf{r}$. The stress created by these two dislocations will cancel to first order at the origin thanks to the symmetry property of the Volterra elastic field.³ As a consequence, this quadrupolar periodic array minimizes the elastic interaction between the dislocations, and hence the Peach-Koehler force acting on each dislocation because of the image dislocations associated with periodic boundaries. It is the best-suited periodic array to extract dislocation core properties from *ab initio* calculations.

Linear elasticity is still used to build the initial configuration, displacing all atoms according to the superposition of the displacement fields created by each dislocation composing the periodic array. The summation on periodic images can be either performed in reciprocal space (Daw 2006) or in direct space after regularization of the conditionally convergent sums (Cai et al 2003). The crystal orientation used in such elastic calculations should be chosen so as to fix the displacement discontinuity exactly in-between the two dislocations composing the dipole, thus preventing the propagation of this discontinuity to infinity. The cut vector \mathbf{A} defining this discontinuity (Fig. 2) is therefore given by $\mathbf{A} = \mathbf{l} \times \mathbf{d}$, where \mathbf{l} is the line vector of the dislocations and \mathbf{d} the vector joining the centers of the $+\mathbf{b}$ dislocation to the $-\mathbf{b}$ one. If the scalar product $\mathbf{A} \cdot \mathbf{b}$ is non-null, *i.e.* if the dislocation dipole has an edge component and the displacement discontinuity does not coincide with the dislocation glide plane, it is also necessary to insert atoms into or delete them from the original lattice at the discontinuity location, thus following the Volterra operation.

A homogeneous strain needs also to be applied to accommodate the plastic strain created by the dipole (Daw 2006; Cai et al 2003) and ensure that the average stress in the simulation cell is null. This can be easily demonstrated by considering the variation of the elastic energy when a homogeneous strain ϵ_{ij} is applied to a simulation cell containing a dislocation dipole defined by its Burgers vector \mathbf{b} and its cut vector \mathbf{A}

$$\Delta E(\epsilon) = \frac{1}{2} S C_{ijkl} \epsilon_{ij} \epsilon_{kl} + C_{ijkl} b_i A_j \epsilon_{kl},$$

where energies are defined per dislocation unit length and have been thus normalized by the height of the simulation cell in the direction of the dislocation line. S is the area of the simulation cell perpendicular to this direction and C_{ijkl} are the elastic constants. The average stress existing in the simulation cell is then given by

$$\sigma_{ij} = \frac{1}{S} \frac{\partial \Delta E}{\partial \epsilon_{ij}} = C_{ijkl} (\epsilon_{kl} - \epsilon_{kl}^0), \quad (2)$$

with the plastic strain defined by

$$\epsilon_{kl}^0 = -\frac{b_i A_j + b_j A_i}{2S}. \quad (3)$$

³ $\sigma_V(-\mathbf{r}) = -\sigma_V(\mathbf{r})$ with σ_V the Volterra stress field of a single dislocation.

One thus sees that the stress given by Eq. 2 is null when the applied strain ε_{ij} is equal to the plastic strain ε_{ij}^0 . When this applied strain is different, a Peach-Koehler force acting on the dislocations may exist. This allows studying properties of the dislocation core under an applied stress, to determine its Peierls stress, for instance. Finally, when a stress variation is observed in *ab initio* calculations, Eq. 2 allows to deduce the plastic strain from this stress, and thus the dislocations' relative positions via the cut vector \mathbf{A} (Eq. 3). For instance, the trajectories of the screw dislocations gliding between two neighbouring Peierls valleys have been determined thanks to this method in HCP Zr (Chaari et al 2014) and in BCC transition metals (Dezerald et al 2016).

With these periodic boundary conditions, all the excess energy contained in the simulation cell is due to the dislocations. As it will be shown in the last section, elasticity theory can be used to isolate the contribution of a single dislocation. These periodic boundary conditions offer thus a convenient way to extract dislocation energy from *ab initio* calculations. But the dislocation core structure, and hence the associated excess energy, can be perturbed by the presence of the periodic images. In practice, one will therefore need to check how sensitive are the obtained dislocation properties with the size of the simulation cell.

4 Dislocation core structures

Different representations can be used to image and analyse the relaxed dislocation core structure obtained by atomic simulations. This allows, for instance, highlighting a spreading of or a dissociation of the dislocation.

4.1 Differential displacement maps

Differential displacement maps were introduced by Vitek et al (1970). Two examples are shown in Fig. 3 for a screw dislocation in a body centered cubic (bcc) crystal and a hexagonal close packed (hcp) crystal. In these maps, the crystal is projected in the plane perpendicular to the dislocation line, using for atomic columns the positions in the perfect crystal. The differential displacement caused by the dislocation is calculated by considering the difference between the vector connecting two neighbour atoms in the relaxed dislocated crystal and the same connecting vector in the perfect crystal. One then plots the projection of this differential displacement along the direction of the Burgers vector with an arrow pointing from one atomic column to the other, centered in the middle of the two columns and with an amplitude proportional to the differential displacement. As the arrows are proportional to the displacement difference, they are a representation of the discrete derivative of the displacement field, *i.e.* of the strain created by the dislocation.

The differential displacement map of the $1/2 \langle 111 \rangle$ screw dislocation in bcc Fe shown in Fig. 3a highlights the compactness and the 3-fold symmetry of the core. Arrows have been normalized so that an arrow linking the centers of two atomic columns corresponds to a differential displacement of $b/3$. One can thus draw Burgers circuits on this map and obtain the norm of the Burgers vector of the enclosed dislocation by summing arrows. The only non-null Burgers vector is obtained for circuits containing the dislocation center indicated by a cross, in particular for the triangle connecting the three central $[111]$ atomic rows, with a norm equal to b . The dislocation is thus well localized.

The picture is quite different for the $1/3 \langle 1\bar{2}10 \rangle$ screw dislocation in hcp Zr shown in Fig. 3b. The differential displacement map shows a non isotropic distribution with a spreading of the dislocation core in the $(10\bar{1}0)$ prismatic plane. The normalization here ensures that the maximal arrows correspond to a $b/2$ differential displacement. The presence of a ribbon with arrows having almost the same length therefore corresponds to a $b/2$ prismatic stacking fault which is known to be stable in this transition metal. The differential displacement map thus clearly evidences the dissociation of the screw dislocation in two $1/6 \langle 1\bar{2}10 \rangle$ partial dislocations separated by a prismatic stacking fault.

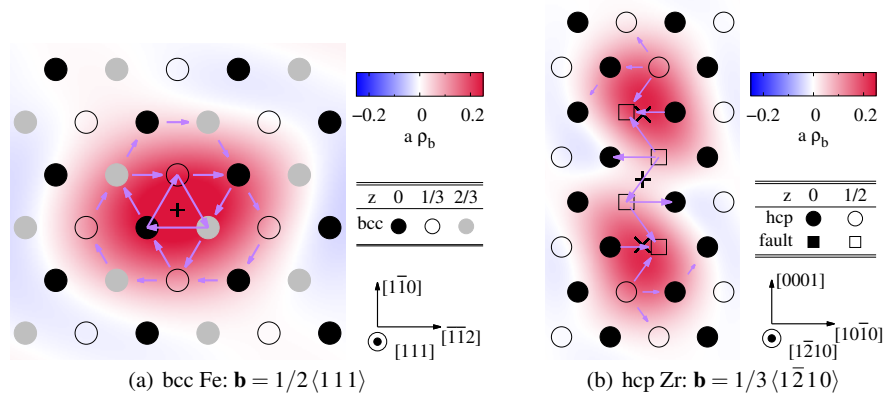


Fig. 3 Core structure of a \mathbf{b} screw dislocation (a) in bcc iron (Dezerald et al 2016) and (b) in hcp zirconium (Clouet et al 2015). In these projections perpendicular to the dislocation line, atoms are sketched by symbols with a colour depending on their (a) (111) and (b) $(1\bar{2}10)$ plane in the original perfect crystal. In (b), different symbols are used for atoms depending on their neighbourhood in the dislocated crystal, *i.e.* close to the perfect hcp crystal (circles) or to the unrelaxed prismatic stacking fault (squares). The arrows between atomic columns are proportional to the differential displacement created by the dislocation in the direction of the Burgers vector. The colour map show the dislocation density ρ_b normalized by the lattice parameter (Nye tensor). The center of the dislocation is indicated by a + cross. The \times crosses in (b) correspond to the positions of the partial dislocations deduced from the disregistry in Fig. 4.

4.2 Dislocation density

Another visualization method proposed by Hartley and Mishin (2005) consists of extracting the Nye tensor from the relaxed atomic structure, thus giving a measure of the dislocation density. The component α_{jk} of the Nye tensor corresponds to the density of dislocations with a line direction along \mathbf{e}_k and a Burgers vector along \mathbf{e}_j . If A is a surface element of normal \mathbf{n} , the dislocation content of line defects along \mathbf{n} intersecting A is given by the surface integral

$$\mathbf{b} = \int_A \boldsymbol{\alpha} \cdot \mathbf{n} dS.$$

We only give here the salient points of the method to extract the Nye tensor from atomic simulations and the reader is referred to the original publication for the practical implementation.

The first step is to define the elastic distortion, *i.e.* the gradient of the elastic displacement, at each atomic position. Note that this differs from the gradient of the total displacement. One cannot simply compare the atomic positions after and before the introduction of the dislocation to obtain this elastic distortion, but one needs to find for each position the closest undistorted environment corresponding to a zero stress state. This is performed by comparing, for each atom, the positions of its nearest neighbours in the dislocated relaxed crystal with the ones in a perfect crystal. Knowing the two sets of neighbour positions, each bond in the dislocated crystal, defined by its vector $\mathbf{P}^{(\gamma)}$, is identified with the corresponding $\mathbf{Q}^{(\beta)}$ bond in the perfect crystal, which is the perfect bond leading to the smallest angle $\Phi^{(\gamma\beta)}$ between the vectors $\mathbf{P}^{(\gamma)}$ and $\mathbf{Q}^{(\beta)}$. Only the bonds which are not too much distorted and for which the angle $\Phi^{(\gamma\beta)}$ is smaller than a chosen threshold are kept. The elastic distortion F^e is then locally defined through the relation $P_i^{(\gamma)} = F_{ij}^e Q_j^{(\beta)}$. This cannot be satisfied for each set of associated bond $(\gamma\beta)$ as the system of equations is overdetermined and the matrix F^e is obtained by the pseudo-inverse method, *i.e.* a least-square fitting. The Nye tensor $\boldsymbol{\alpha}$ is then defined through the rotational of the inverse transpose of the distortion, $\boldsymbol{\alpha} = -\nabla \times (F^e)^{-1}$, using finite differences between neighbour atoms for derivation. This defines the Nye tensor on a set of discrete points, generally atomic positions, which can be then interpolated with cubic-splines or Fourier series, or smeared with Gaussian-like spreading functions.

The dislocation density obtained for the $1/2\langle 111 \rangle$ screw dislocation in bcc Fe (Fig. 3a) illustrates the compactness of the core: the distribution has only one peak. On the other hand, the dislocation distribution for the $1/3\langle 1\bar{2}10 \rangle$ screw dislocation in hcp Zr (Fig. 3b) shows two well-separated peaks which correspond to the two partial dislocations. To obtain the Nye tensor in this latter case, the neighbourhood of each atom in the dislocated crystal is compared not only to the two different neighbourhoods existing in the perfect hcp crystal, but also to the ones of the unrelaxed prismatic stacking fault, to identify the closer reference from which the elastic distortion is calculated.

4.3 Disregistry

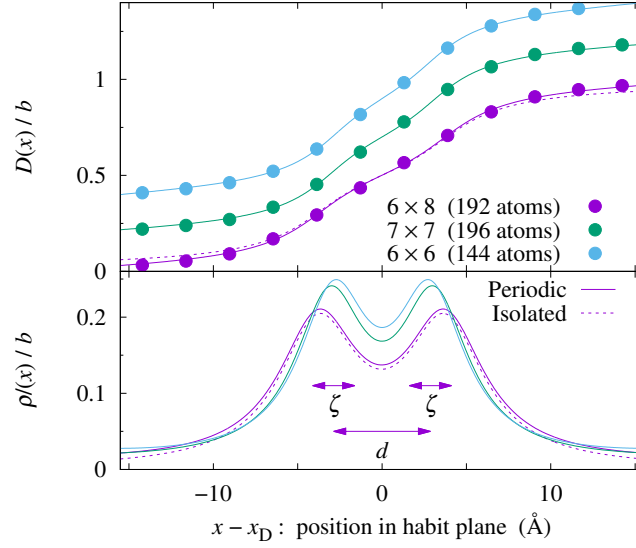


Fig. 4 Disregistry $D(x)$ created by a $1/3 \langle 1\bar{2}10 \rangle$ screw dislocation in its $(10\bar{1}0)$ prismatic glide plane in hcp Zr, and corresponding dislocation density $\rho(x) = \partial D(x)/\partial x$. Symbols correspond to *ab initio* calculations and lines to the fit of the Peierls-Nabarro model, considering periodicity or not (straight and dashed lines respectively). Results are shown for different $n \times m$ periodic arrangements corresponding to the periodicity vectors $\mathbf{u}_1 = n/2 [10\bar{1}0]$ and $\mathbf{u}_2 = m [0001]$ (see Clouet (2012) for details). For clarity, disregistries $D(x)$ have been shifted by 0.2 between different data sets. The obtained dissociation distance d and spreading ζ of the partial dislocations are indicated for the 6×8 periodic array whose core structure is shown in Fig. 3b.

The extraction of the disregistry offers another way to characterize the dislocation core structure, particularly convenient when the core is planar. The disregistry is the difference of displacement induced by the dislocation between the plane just above and the one just below the dislocation glide plane. It is thus obtained from the relaxed configuration through

$$\mathbf{D}(x) = \mathbf{u}^+(x) - \mathbf{u}^-(x),$$

where $\mathbf{u}^+(x)$ and $\mathbf{u}^-(x)$ are the displacements of the atoms belonging respectively to the upper and lower planes and located at the position x in the direction perpen-

dicular to the dislocation line. This disregistry varies⁴ from $\mathbf{0}$ for $x \rightarrow -\infty$ to \mathbf{b} for $x \rightarrow \infty$, thus corresponding to the dislocation glide plane being locally sheared by one Burgers vector \mathbf{b} . The dislocation center x_D is defined by $\mathbf{D}(x_D) = \mathbf{b}/2$. The disregistry derivative, $\rho(x) = \partial \mathbf{D}(x)/\partial x$, corresponds to the dislocation density in the glide plane.

Peierls and Nabarro built a model that leads to a simple analytical expression of the disregistry (Lu 2005). According to this model, the disregistry⁵ is given by

$$D(x) = \frac{b}{\pi} \left[\arctan \left(\frac{x - x_D}{\zeta} \right) + \frac{\pi}{2} \right],$$

where x_D is the dislocation position and ζ its spreading in the glide plane. Fitting of these two parameters to the data extracted from the atomistic simulations allows thus defining the dislocation position and characterizing the spreading of its core.

For dissociated dislocations, the disregistry is the sum of the contributions of the two partial dislocations, *i.e.*, assuming that each partial dislocation has the same Burgers vector $\mathbf{b}/2$ and the same spreading ζ ,

$$D(x) = \frac{b}{2\pi} \left[\arctan \left(\frac{x - x_D - d/2}{\zeta} \right) + \arctan \left(\frac{x - x_D + d/2}{\zeta} \right) + \pi \right],$$

where d is the dissociation distance. As shown in Fig. 4 for the $1/3 \langle 1\bar{2}10 \rangle$ screw dislocation in hcp Zr, such an analytical expression generally perfectly describes the disregistry extracted from the atomic simulations. One can also notice that the positions in the glide plane of the partial dislocations deduced from the disregistry agree with what can be inferred from the differential displacement and the Nye tensor maps (Fig. 3b). Some consequences of the periodic boundary conditions used to model this dislocation are visible on these disregistry plots. The dislocation density slightly depends, through the dissociation distance d and the partial spreading ζ , on the simulation cell, not only its size but also its shape. One also sees that the density of the periodic dislocation arrays (solid line in Fig. 4), obtained by summation of the contributions of the periodic images in the glide plane, slightly differs from the one of the isolated dislocation (dashed line in Fig. 4), especially in the distribution tail. Flexible boundary conditions, as discussed in Section 3.2, have been developed to solve such limitations of periodic boundary conditions.

⁴ If the cut plane used to introduce the dislocation in the simulation cell does not correspond to its glide plane, it is necessary to define the atomic displacement in the $\mathbf{0}$ to \mathbf{b} interval. This can be done as the Burgers vector \mathbf{b} of a perfect dislocation is a periodicity vector of the lattice and adding a displacement $n\mathbf{b}$ ($n \in \mathbb{Z}$) to an atom does not change the configuration.

⁵ For simplicity, we consider scalar quantities by projecting the displacement in the direction of the Burgers vector.

5 Dislocation energy

Ab initio calculations give access to the dislocation core energy and its variations. This core energy is the part of the dislocation excess energy which arises from the strong perturbation of the atomic interactions in the immediate vicinity of the dislocation line and which cannot be described by linear elasticity. Contrary to the dislocation elastic energy, this is an intrinsic property which only depends on the dislocation and not on the surrounding environment. When several configurations exist for the same dislocation, this core energy controls their relative stability. Its variations with the position of the dislocation in the crystal lattice is at the origin of the lattice friction opposing dislocation glide.

5.1 Core energy

Among the different boundary conditions introduced in section 3 to model a dislocation at an atomic scale, only periodic boundary conditions allow for an unambiguous determination of the dislocation core energy with *ab initio* calculations. This is a consequence of the energy formulation inherent to *ab initio* calculations. Because of the non-locality of the electronic energy, which contains a contribution which needs to be evaluated in reciprocal space, one cannot easily partition the excess energy of the simulation cell between the dislocation and the external boundary contributions when a defective boundary has been introduced like in cluster approaches using either fixed (§ 3.1) or flexible boundaries (§ 3.2). *Ab initio* methods to project the energy on atoms have been proposed: they theoretically allow for such a partition but the application to the calculation of a dislocation core energy still remains to be done. Even if the absolute value of the core energy appears difficult to determine with cluster approaches, methods to estimate its variation are nevertheless possible. One can, for instance, calculate the difference of core energy between two configurations of the same dislocations by simply considering the difference of *ab initio* total energies. But such an approach assumes that the contribution of the external boundary will cancel in the difference, an assumption which may be hard to validate. Variation of the dislocation energy with its position in the crystal lattice can also be estimated by considering the work of the atomic forces during the motion (Swinburne and Kermode (2017)).

On the other hand, with periodic boundary conditions, all the excess energy arises from the dislocations. This excess energy ΔE is defined as the energy difference per unit of height between the supercell with and without the dislocation dipole.⁶ It is given by the sum of the core energy E^{core} of the two dislocations, of the elastic energy $E_{\text{dipole}}^{\text{elas}}$ of the dipole contained in the supercell and of its elastic interaction with its periodic images:

⁶ If atoms have been removed or inserted during the creation of the dipole, the energy of the perfect supercell needs to be normalized by the correct number of atoms.

$$\Delta E = 2E^{\text{core}} + E_{\text{dipole}}^{\text{elas}} + \frac{1}{2} \sum_{n,m} E_{\text{inter}}^{\text{elas}}(n\mathbf{u}_1 + m\mathbf{u}_2). \quad (4)$$

The factor $1/2$ appears in front of this last contribution as only one half of the interaction is attributed to each interacting dipole. When partitioning the excess energy into a core and an elastic contribution, it is necessary to introduce a cutoff distance to isolate the dislocation cores. Close to the dislocation lines, strains are much too high to be described by linear elasticity. As a consequence, elastic fields diverge at the origin and one needs to exclude the core region from the elastic description. The elastic contribution to the excess energy is thus obtained by integrating the elastic energy density on the whole supercell except two cylinders of radius r_c which isolate this elastic divergence. The core energy corresponds to the excess energy contained in these cylinders. The total excess energy ΔE does not depend on the choice for this core radius, but the partition between a core and an elastic contribution depends on r_c .

The elastic energy of the dipole and its interaction with its periodic images can be computed by considering the Volterra elastic field created by the dislocations. This calculation can be performed either in reciprocal space (Daw 2006) or in direct space using classical results of dislocation elastic theory (Bacon et al 1980). In this last case, one uses the decomposition of Eq. (4), with the contribution of the dipole contained in the supercell and its interaction with the periodic images calculated separately. The dipole elastic energy is obtained by the volume integral

$$E_{\text{dipole}}^{\text{elas}} = \frac{1}{2} \iiint_V \left(\sigma_{ij}^{(1)} + \sigma_{ij}^{(2)} \right) \left(\epsilon_{ij}^{(1)} + \epsilon_{ij}^{(2)} \right) dV,$$

where $\sigma^{(n)}$ and $\epsilon^{(n)}$ are the stress and strain created by the dislocation n . This is transformed into a surface integral thanks to Gauss' theorem

$$E_{\text{dipole}}^{\text{elas}} = \frac{1}{2} \iint_S \left(\sigma_{ij}^{(1)} + \sigma_{ij}^{(2)} \right) \left(u_i^{(1)} + u_i^{(2)} \right) dS_j,$$

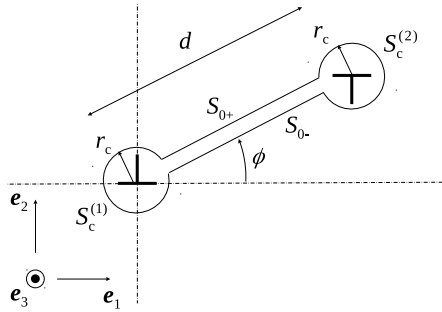


Fig. 5 Definition of the contour surface used to calculate the elastic energy of a dislocation dipole

with $\mathbf{u}^{(n)}$ the displacement field associated with dislocation n . The integration surface is composed of the two cylinders $S_c^{(1)}$ and $S_c^{(2)}$ of radii r_c removing the elastic divergence at the dislocation cores, and of the two surfaces S_{0-} and S_{0+} removing the displacement discontinuity along the dislocation cut (Fig. 5). The integration on both core cylinders leads to the same contribution

$$E_c^{\text{elas}}(\phi) = \frac{1}{2} \iint_{S_c^{(1)}} \sigma_{ij}^{(1)} u_i^{(1)} dS_j = \frac{1}{2} \iint_{S_c^{(2)}} \sigma_{ij}^{(2)} u_i^{(2)} dS_j. \quad (5)$$

This contributions of the core tractions to the elastic energy (Clouet 2009) should not be forgotten as it ensures that the elastic energy is a state variable compatible with the work of the Peach-Koehler forces. Besides, in *ab initio* calculations where the distance d between the two dipole dislocations is small, this can lead to a non negligible contribution compared to the one associated with the integral along the cut surface, even for a screw orientation. The elastic energy of the dislocation dipole is then

$$E_{\text{dipole}}^{\text{elas}} = 2E_c^{\text{elas}}(\phi) + b_i K_{ij}^0 b_j \ln \left(\frac{d}{r_c} \right), \quad (6)$$

where the tensor \mathbf{K}^0 defined by Stroh (1958, 1962) only depends on the elastic constants. The total elastic energy is finally obtained by adding the interaction of the dipole with its periodic images. But, one should realize that the summation on periodic images appearing in Eq. (4) is only conditionally convergent: it can be regularized with the method of Cai et al (2003).

As shown in Fig. 6 for the $1/2 \langle 111 \rangle$ screw dislocation in bcc iron, once this elastic energy is subtracted from the dislocation excess energy given by *ab initio*

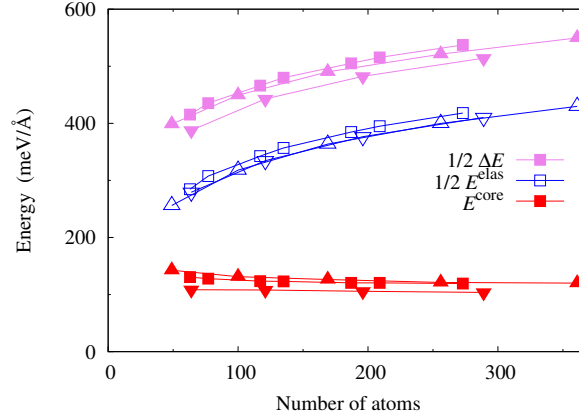


Fig. 6 Decomposition of the excess energy ΔE of a $1/2 \langle 111 \rangle$ screw dislocation dipole in bcc Fe in an elastic contribution E^{elas} and a core energy E^{core} , using a core radius $r_c = b/2$. Different symbols correspond to different periodic arrangements (see Clouet et al (2009) for details).

calculations, one obtains a constant core energy which does not depend on the size of the supercell. Some slight variations of the core energy are nevertheless still observed with the type of periodic arrangement used for the atomic simulations. These variations arise because only the Volterra elastic field has been considered in the calculation of the elastic energy. Dislocations also cause a core elastic field, which decays more rapidly than the Volterra elastic field. Because of the small size of the supercell used in *ab initio* calculations, this core field may also lead to an elastic interaction between the different dislocations composing the periodic array. This contribution to the elastic energy can be computed to improve the convergence of core energies (Clouet et al 2009). A quadrupolar periodic arrangement minimizes this contribution of the core field. This is why such an arrangement is preferred when periodic boundary conditions are used. The neglect of anharmonic effects in the calculation of the elastic energy can also be a reason for the variation of the core energy with the supercell. Knowing higher order elastic constants, one can use non-linear elasticity theory in principle to calculate more precisely this elastic contribution (Teodosiu 1982). But this leads to much cumbersome calculations. In practice, as anharmonicity is important only close to the dislocation core, the consideration of the dislocation core field offers a way to incorporate anharmonic effects while still relying on linear elasticity.

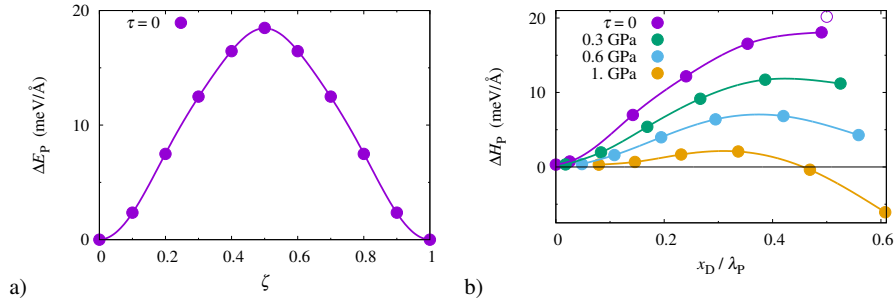


Fig. 7 Peierls barrier of a $1/2\langle 111 \rangle$ screw dislocation in bcc Mo. (a) The energy variation ΔE is shown as a function of the reaction coordinate ζ , and (b) the enthalpy variation ΔH as a function of the dislocation position x_D normalized by the distance λ_P between two Peierls valleys (see Dezerald et al (2014, 2016) for details). For the Peierls barriers under stress (b), only one half of the barrier has been computed, with one dislocation of the dipole being displaced while the second one remains fixed. The open symbol is the enthalpy variation in the middle of the pathway ($x_D/\lambda_P = 1/2$) before correcting for the variation of the elastic interaction energy for the $\tau = 0$ calculation.

5.2 Peierls energy barrier

The Peierls energy is the energy barrier opposing dislocation glide. It corresponds to a variation of the dislocation core energy as the elastic energy is not dependent upon the dislocation position in the crystal lattice. It can be calculated by finding the minimum energy path linking two neighbouring stable positions of the dislocation using either constrained minimization or nudged elastic band (NEB) calculations (Henkelman et al 2000).

With periodic boundary conditions, the Peierls energy is directly obtained by considering a path where both dislocations composing the dipole are displaced by one Peierls valley in the same direction. If the two dislocations are moved simultaneously along the path, their separation distance does not vary and the elastic energy is constant. This ensures that the energy variation given by the constrained minimization or the NEB calculations directly corresponds to the Peierls energy. However, this is possible only if crystal symmetry ensures that the path is symmetrical as the two dislocations are traversing their Peierls barriers in the opposite direction. This is the case, for instance, for the $1/2 \langle 111 \rangle$ screw dislocation in a bcc lattice gliding in a $\{110\}$ plane (Fig. 7a).

If the path is not symmetrical, either because of the lack of crystal symmetries or because of an applied stress, it is not possible anymore to move both dislocations simultaneously in the same direction. One needs either to move them in opposite directions or to keep one dislocation fixed when the second one is moving. As a consequence, the separation distance, and thus the elastic interaction energy, is varying along the path. One can calculate this variation of the elastic energy and subtract it from the excess energy in order to obtain the Peierls energy. To be able to perform this elastic calculation, one needs first to determine the exact dislocation position x_D for each reaction coordinate ζ along the path. This can be done using the dislocation registry (*cf.* §4.3) if the motion is planar or by fitting the atomic displacements with the Volterra elastic solution. As the stress is directly linked to the applied strain and the dislocation positions (Eqs. 2 and 3), one can also use the stress variation observed along the dislocation path to determine the dislocations position. The example of Fig. 7b shows that, with this correction for the variation of the elastic energy, the same Peierls energy is obtained under zero applied stress when one dislocation is fixed or when both dislocations are moved (Fig. 7a).

5.3 Peierls stress

The Peierls stress is the applied resolved shear stress necessary to cancel the Peierls barrier so that the dislocations can glide freely without the need of thermal activation, *i.e.* the stress necessary to move the dislocation at 0 K. For an applied stress τ , the Peierls barrier is given by the enthalpy variation

$$\Delta H_P(x_D, \tau) = \Delta E_P(x_D) - \tau b x_D,$$

which corresponds to the Peierls energy barrier plus the work of the applied stress when the dislocation has glided a distance x_D . The Peierls stress is thus the maximum applied stress τ for which the function $\Delta H_P(x_D, \tau)$ goes through a maximum in the range $0 \leq x_D \leq \lambda_P$. If one assumes that the energy barrier $\Delta E_P(x_D)$ does not depend on the applied stress τ , it is given by

$$\tau_P = \frac{1}{b} \text{Max} \left(\frac{\partial \Delta E_P}{\partial x_D} \right). \quad (7)$$

The Peierls stress can thus be theoretically obtained from the calculation of the Peierls energy barrier under zero applied stress. But, the evaluation of the derivative in Eq. 7 requires to know the variation of the energy as a function of the dislocation position and not only of the reaction coordinate. In practice, the obtained value for τ_P will sensitively vary with the method chosen to estimate the dislocation position along the path.

One can also directly calculate with *ab initio* calculations the Peierls barrier under an applied stress so as to estimate at which stress the barrier cancels (Fig. 7). In such calculations, one does not really apply a stress but a strain corresponding to the target stress (Eq. 2). With periodic boundary conditions, as the distance between the two dislocation is varying, the applied stress is also varying along the path. Eqs. (2) and (3) show that the stress variation is directly proportional to the dislocation displacement and to the inverse of the surface S of the simulation cell perpendicular to the dislocation line. If only one dislocation is moving along the path, this stress variation therefore does not exceed

$$\delta \tau = \mu \frac{b \lambda_P}{S},$$

where μ is the shear modulus in the dislocation glide plane.

If one is only interested in the calculation of the Peierls stress and not in the variation of the Peierls barrier with the applied stress, one can simply perform static relaxation of a dislocation under an applied stress to see at which applied stress the dislocation glides by at least one Peierls valley. With periodic boundary conditions one still needs to take into account the variation of the elastic interaction and of the applied stress when the dislocation is moving to interpret the results. On the other hand, no such artifact exists with a cluster approach using flexible boundary conditions which truly models a single isolated dislocation under an applied stress. Straining homogeneously the simulation cell to obtain the targeted applied stress, the Peierls stress is defined as the stress for which the dislocation cannot be stabilized anymore and escapes from the cluster. If one is only interested in the evolution of the dislocation core structure under an applied stress and on the determination of the Peierls stress, this cluster approach therefore appears as the method of choice. Nevertheless, whatever the boundary conditions, determination of the Peierls stress by such an instability condition of the dislocation core under an applied stress necessitates a strict threshold criterion on the atomic forces to obtain a meaningful value.

6 Conclusions

Dislocation core properties can now be routinely studied with *ab initio* calculations thanks to the different methodological developments summarized in this chapter. This usually necessitates a coupling between atomistic model and elasticity theory, for which different already available tools can be used: see, for instance, D. R. Trinkle website⁷ for an implementation of the lattice Greens functions or the Babel package⁸ for handling dislocations in atomistic simulation cells and elastic energy calculations. Useful information on the dislocation core structure are thus obtained. Such calculations can, for instance, characterize possible dissociation or spreading of the core, or evidence the existence of several stable configurations for the same dislocation. One gets access to the different energy barriers opposing the dislocation motion and to their variation with the applied stress. It is also possible to study how these core properties are altered by the interaction with solute atoms.

Because of the limited size that can be handled by *ab initio* calculations, such studies are usually limited to the study of straight dislocation, and only few *ab initio* calculations have considered until now the presence of kinks on the dislocation lines. Upscaling modeling approaches, relying, for instance, to the line tension approximation to describe kink nucleation, are therefore needed to go from these fundamental core properties determined at 0 K with *ab initio* calculations to dislocation mobility laws at finite temperature. Larger atomistic simulations are also possible using empirical potentials to describe atomic interactions. These simulations allow studying more complex situations and simulating different dislocation mechanisms, like glide, cross-slip and interaction with other elements of the microstructure, without assuming *a priori* the elementary mechanism. In such a context, *ab initio* calculations are useful to validate and also help the development of empirical potentials which correctly reproduce dislocation fundamental properties.

Acknowledgements Drs. Nermine Chaari, Lucile Dezerald, and Lisa Ventelon are acknowledged for their contributions to the works presented here. Dr. Antoine Kraych is thanked for fruitful discussions. Parts of this work have been performed using HPC resources from GENCI-CINES and -TGCC (Grant 2017-096847).

References

- Bacon DJ, Barnett DM, Scattergood RO (1980) Anisotropic continuum theory of lattice defects. *Prog Mater Sci* 23:51–262, doi:10.1016/0079-6425(80)90007-9
- Cai W, Bulatov VV, Chang J, Li J, Yip S (2003) Periodic image effects in dislocation modelling. *Philos Mag* 83:539–567, doi:10.1080/0141861021000051109
- Chaari N, Clouet E, Rodney D (2014) First-principles study of secondary slip in zirconium. *Phys Rev Lett* 112:075,504, doi:10.1103/PhysRevLett.112.075504

⁷ <http://dtrinkle.matse.illinois.edu>

⁸ <http://emmanuel.clouet.free.fr/Programs/Babel>

- Chen Q, Liu XY, Biner S (2008) Solute and dislocation junction interactions. *Acta Mater* 56:2937–2947, doi:10.1016/j.actamat.2008.02.026
- Choly N, Lu G, E W, Kaxiras E (2005) Multiscale simulations in simple metals: A density-functional-based methodology. *Phys Rev B* 71:094,101, doi:10.1103/physrevb.71.094101
- Clouet E (2009) Elastic energy of a straight dislocation and contribution from core tractions. *Philos Mag* 89:1565–1584, doi:10.1080/14786430902976794
- Clouet E (2012) Screw dislocation in zirconium: An ab initio study. *Phys Rev B* 86:144,104, doi:10.1103/PhysRevB.86.144104
- Clouet E, Ventelon L, Willaime F (2009) Dislocation core energies and core fields from first principles. *Phys Rev Lett* 102:055,502, doi:10.1103/PhysRevLett.102.055502
- Clouet E, Caillard D, Chaari N, Onimus F, Rodney D (2015) Dislocation locking versus easy glide in titanium and zirconium. *Nat Mater* 14:931–936, doi:10.1038/nmat4340
- Daw MS (2006) Elasticity effects in electronic structure calculations with periodic boundary conditions. *Comp Mater Sci* 38:293–297, doi:10.1016/j.commatsci.2006.02.009
- Dezerald L, Ventelon L, Clouet E, Denoual C, Rodney D, Willaime F (2014) Ab initio modeling of the two-dimensional energy landscape of screw dislocations in bcc transition metals. *Phys Rev B* 89:024,104, doi:10.1103/PhysRevB.89.024104
- Dezerald L, Rodney D, Clouet E, Ventelon L, Willaime F (2016) Plastic anisotropy and dislocation trajectory in BCC metals. *Nat Commun* 7:11,695, doi:10.1038/ncomms11695
- Eshelby JD, Read WT, Shockley W (1953) Anisotropic elasticity with applications to dislocation theory. *Acta Metall* 1:251–259, doi:10.1016/0001-6160(53)90099-6
- Hartley CS, Mishin Y (2005) Characterization and visualization of the lattice misfit associated with dislocation cores. *Acta Mater* 53:1313–1321, doi:10.1016/j.actamat.2004.11.027
- Henkelman G, Jóhannesson G, Jónsson H (2000) Methods for finding saddle points and minimum energy paths: theoretical methods in condensed phase chemistry. In: Schwartz SD (ed) *Progress in Theoretical Chemistry and Physics*, vol 5, Springer Netherlands, chap 10, pp 269–302, doi:10.1007/0-306-46949-9_10
- Hirth JP, Lothe J (1982) *Theory of Dislocations*, 2nd edn. Wiley, New York
- Hohenberg P, Kohn W (1964) Inhomogeneous electron gas. *Phys Rev* 136:B864–B871, doi:10.1103/PhysRev.136.B864
- Kohn W, Sham LJ (1965) Self-consistent equations including exchange and correlations effects. *Phys Rev* 140:A1133–A1138, doi:10.1103/PhysRev.140.A1133
- Liu Y, Lu G, Chen Z, Kiousis N (2007) An improved QM/MM approach for metals. *Modelling Simul Mater Sci Eng* 15:275–284, doi:10.1088/0965-0393/15/3/006
- Lu G (2005) The Peierls-Nabarro model of dislocations: a venerable theory and its current development. In: Yip S (ed) *Handbook of Materials Modeling*, Springer, The Netherlands, chap 2.20, pp 793–811
- Rao S, Hernandez C, Simmons JP, Parthasarathy TA, Woodward C (1998) Green's function boundary conditions in two-dimensional and three-dimensional atomistic simulations of dislocations. *Philos Mag A* 77:231–256, doi:10.1080/01418619808214240
- Rodney D, Ventelon L, Clouet E, Pizzagalli L, Willaime F (2017) Ab initio modeling of dislocation core properties in metals and semiconductors. *Acta Mater* 124:633–659, doi:10.1016/j.actamat.2016.09.049
- Segall DE, Strachan A, Goddard WA, Ismail-Beigi S, Arias TA (2003) Ab initio and finite-temperature molecular dynamics studies of lattice resistance in tantalum. *Phys Rev B* 68:014,104, doi:10.1103/PhysRevB.68.014104
- Sinclair JE, Gehlen PC, Hoagland RG, Hirth JP (1978) Flexible boundary conditions and nonlinear geometric effects in atomic dislocation modeling. *J Appl Phys* 49:3890–3897, doi:10.1063/1.325395
- Stroh AN (1958) Dislocations and cracks in anisotropic elasticity. *Philos Mag* 3:625–646, doi:10.1080/14786435808565804
- Stroh AN (1962) Steady state problems in anisotropic elasticity. *J Math Phys (Cambridge, Mass)* 41:77

- Swinburne TD, Kermode JR (2017) Computing energy barriers for rare events from hybrid quantum/classical simulations through the virtual work principle. *Phys Rev B* 96:144,102, doi:10.1103/PhysRevB.96.144102
- Tan AMZ, Trinkle DR (2016) Computation of the lattice Green function for a dislocation. *Phys Rev E* 94:023,308, doi:10.1103/PhysRevE.94.023308
- Teodosiu C (1982) *Elastic Models of Crystal Defects*. Springer-Verlag, Berlin
- Vitek V, Perrin RC, Bowen DK (1970) The core structure of $1/2\langle 111 \rangle$ screw dislocations in b.c.c. crystals. *Philos Mag* 21:1049–1073, doi:10.1080/14786437008238490
- Woodward C (2005) First-principles simulations of dislocation cores. *Mater Sci Eng A* 400-401:59–67, doi:10.1016/j.msea.2005.03.039
- Yasi JA, Hector LG, Trinkle DR (2012) Prediction of thermal cross-slip stress in magnesium alloys from a geometric interaction model. *Acta Mater* 60:2350–2358, doi:10.1016/j.actamat.2012.01.004